Chaotic scattering off the magnetic dipole

1988 J. Phys. A: Math. Gen. 21 2301

(http://iopscience.iop.org/0305-4470/21/10/010)

J. Phys. A: Math. Gen. **21** (1988) 2301-2311. Printed in the UK

Chaotic scattering off the magnetic dipole

Christof Jung and Hans-Joachim Scholz

Fachbereich Physik der Universität Bremen, D-2800 Bremen 33, Federal Republic of Germany

Received 19 November 1987

Abstract. Classical scattering with singularities of Cantor-set type can be observed if unstable localised orbits exist whose homoclinic structures are transported to infinity by the Hamiltonian flow. An electron moving in the field of a magnetic dipole is a simple example of physical relevance to demonstrate this transport mechanism. In the asymptotic plane spanned by impact parameter and incoming direction the deflection function is singular for initial conditions leading to captured orbits. Using the method of Poincaré sections, we find a correspondence between this set of singularities and the stable manifolds of localised orbits. The scattering data which are measured in the asymptotic region of free motion provide information about chaotic motion in a finite part of the position space.

1. Introduction

In recent years much work has been done on chaos in bound classical Hamiltonian systems. Meanwhile it is well known how chaos shows up in these systems, and powerful methods have been applied to investigate their behaviour. In contrast, the physical understanding of chaos in classical scattering systems is less developed.

From the mathematical point of view it has been shown that topological chaos can exist on non-compact energy surfaces due to the interplay of homoclinic and heteroclinic connections of periodic bound orbits (Churchill *et al* 1979). For nearly twenty years there have been numerical observations of complicated behaviour in classical models for inelastic molecular scattering (Rankin and Miller 1971, Gottdiener 1975, Fitz and Brumer 1979, Agmon 1982, Schlier 1983, Noid *et al* 1986). More recently, chaos has been found in satellite encounters (Petit and Henon 1986), in vortex dynamics (Eckhardt 1988, Eckhardt and Aref 1988) and in potential scattering (Eckhardt and Jung 1986, Jung and Scholz 1987). In this paper we investigate in more detail how scattering properties are influenced by chaotic structures positioned in a localised region of phase space which can be reached from infinity by the Hamiltonian flow.

As a simple and physically relevant example we treat the classical scattering of an electrically charged particle in the field of a magnetic dipole, the so-called Stormer problem. As shown by Braun (1970), Contopoulos and Vlahos (1975) and Dragt and Finn (1976) this system is not completely integrable and exhibits chaotic bound trajectories.

In § 2 we determine periodic orbits by iterating symmetry lines of an appropriate Poincaré map. The invariant manifolds of the most important fixed point are constructed in § 4 to explain the singularities of the deflection function presented in § 3. The global structure of the singularity set is treated in § 5 by transporting the coordinate lattice of the asymptotic region into the Poincaré plane.

0305-4470/88/102301+11$02.50

In the following we call a point in the set of initial conditions singular, if the deflection function is discontinuous and the time delay function becomes infinite at this point.

2. Finding periodic orbits

The motion of an electrically charged particle in the field of a magnetic dipole is determined by the Hamiltonian

$$H = (\boldsymbol{p} - Q\boldsymbol{A}/c)^2/2m \tag{1}$$

where

$$\boldsymbol{A} = A_0(-y/r^3, x/r^3, 0).$$

Here we have used the following notation: x, y, z denote cartesian coordinates in position space, $r^2 = x^2 + y^2 + z^2$, $\boldsymbol{p}$ is the momentum, m is the mass and Q is the electric charge of the particle. The strength of the magnetic dipole is given by A_0. Because of the rotational symmetry of the magnetic field it is convenient to introduce cylindrical coordinates ρ, φ, z and conjugate momenta p_ρ, p_φ, p_z where p_φ is a conserved quantity. Assuming $p_\varphi > 0$ and adopting the scaling of Dragt and Finn (1976) equation (1) can be reduced to the following Hamiltonian system with two degrees of freedom:

$$H = \tfrac{1}{2}(p_\rho^2 + p_z^2) + V(\rho, z) \tag{2}$$

$$V(\rho, z) = \tfrac{1}{2}(1/\rho - \rho/r^3)^2. \tag{3}$$

Some contour lines of the potential (3) are shown in figure 1. On the curve $\rho^2 = r^3$, called the 'thalweg', the potential takes its minimal value zero. At $P_S = (2, 0)$ there is a saddle point with height $V = E_S = \frac{1}{32}$. For $\rho \to \infty$ the potential vanishes. For $\rho \to 0$ the potential tends to infinity except along the thalweg where V is identically zero.

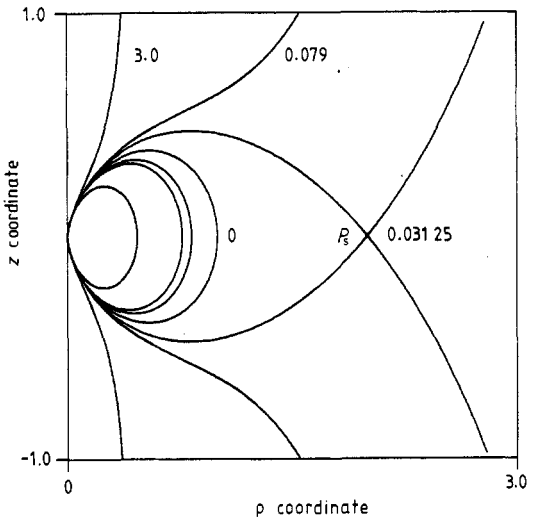

Figure 1. Contour lines of the potential (3) for $V = 0, \frac{1}{32}, 0.079, 3$ (ρ, horizontal axis; z, vertical axis)

Since scattering chaos originates from unstable periodic orbits (Churchill *et al* 1979, Jung and Scholz 1987) we start our investigation by looking for simple periodic orbits with energy $E > E_S$. At $E = E_S$ we can linearise around the saddle point to find a periodic orbit γ oscillating back and forth on the ridge of the potential mountain. The continuation of γ for $E > E_S$ can be found numerically by the following method: let M be the Poincaré map in the $\rho - \dot{\rho}$ plane F defined by $z = 0$, $\dot{z} > 0$. Let σ be the line $\dot{\rho} = 0$. Using the fact that the Hamiltonian (2) is invariant under time reversal $t \to -t$ and under spatial reflection $z \to -z$ one can show that the intersection $M(\sigma) \cap \sigma$ contains points of period one or two. Not all points $P \in F$ have an image $M(P)$. There are orbits starting with $z = 0$, $\dot{z} > 0$, escaping to infinity and never hitting the plane $z = 0$ again. In figure 2 only that part of the symmetry line is shown whose Poincaré image exists. For $E = 0.05$, for example, this part consists of two disjoint components.

There exists a bifurcation energy $E_M \approx 0.08$, with the following properties: for $E > E_M$ the intersection $M(\sigma) \cap \sigma$ is empty (see figure 2(*a*)). At energy $E = E_M$ a saddle node bifurcation occurs creating an elliptic fixed point P_e and a hyperbolic fixed point P_h which turns out to represent the oscillating orbit γ. The eigenvalues λ_1 and $\lambda_2 = 1/\lambda_1$ of P_h are equal to 1 at the bifurcation energy E_M. With energy decreasing down to E_S the eigenvalue λ_1 increases monotonically. Finally, at $E = E_S$ the fixed point P_h vanishes with

$$\lambda_1 = \exp\left\{2\pi\left[-\frac{\partial^2 V}{\partial \rho^2}\bigg|_{P_S}\left(\frac{\partial^2 V}{\partial z^2}\bigg|_{P_S}\right)^{-1}\right]^{1/2}\right\}$$
$$= \exp[2\pi(2/3)^{1/2}] \approx 170.$$

Obviously, for $E < E_S$ the orbit γ cannot exist.

In figure 2(*b*), $E = 0.079$, the curves σ and $M(\sigma)$ intersect at P_e almost tangentially. For $E \approx 0.078$ this elliptic point breaks up into three points of intersection which bifurcate again at lower energies, see figure 2(*c*). Not all periodic points of M can

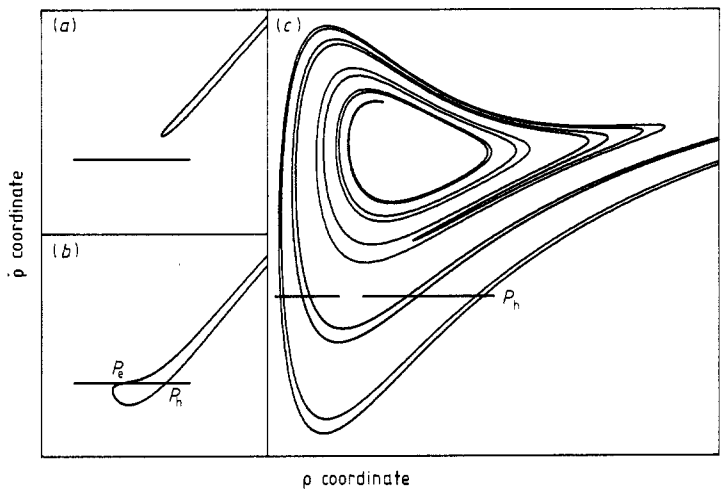

Figure 2. The symmetry line $\dot{\rho} = 0$ and its Poincaré image in the $\rho/\dot{\rho}$ plane $z = 0$, $\dot{z} > 0$. In (*a*) and (*b*) the frame is $\rho \in [0.8, 1.5]$ (horizontal axis); $\dot{\rho} \in [-0.05, 0.1]$ (vertical axis). In (*c*) the frame is $\rho \in [0.8, 2.5]$ (horizontal axis); $\dot{\rho} \in [-0.18, 0.32]$ (vertical axis). (*a*) $E = 0.082$; (*b*) $E = 0.079$; (*c*) $E = 0.05$.

be found by the method of intersecting the symmetry line and its image. However, in the following we will see that the orbit γ suffices to explain the main features of the scattering singularities.

3. Singularities of the deflection function

In this section we present the chaotic effects appearing in the deflection function

$$D(\alpha, b, E) = \beta - \alpha + \pi$$

where $\alpha = \tan^{-1}(p_{z\,\mathrm{in}}/p_{\rho\,\mathrm{in}})$ and $\beta = \tan^{-1}(p_{z\,\mathrm{out}}/p_{\rho\,\mathrm{out}})$ are the directions of the incoming and outgoing momentum, respectively. The incoming particle starts with impact parameter

$$b = z - \rho \tan \alpha.$$

In addition, it is interesting to consider the time delay

$$T(\alpha, b, E) = T_a - T_h$$

between the actual motion and the motion that would occur for scattering off a hard wall at $\rho = 0$. In figures 3-5 the deflection angle and the time delay are plotted for fixed energy and $\alpha = \pi$ as a function of b. Due to the symmetry of the potential we have $D(b) = -D(-b)$ and $T(b) = T(-b)$ for $\alpha = \pi$. The functions D and T show singularities for $E \in (E_S, E_M)$. For $E < E_S$ the particle cannot enter the relevant potential region; for $E > E_M$ there is no periodic orbit to capture the particle.

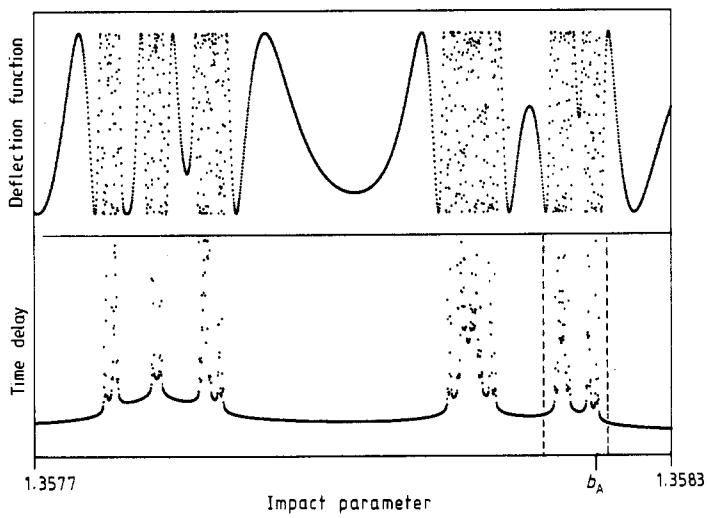

Figure 3. The deflection function $D(b)$ (upper frame) and the time delay $T(b)$ (lower frame) for energy $E = 0.079$ and incoming direction $\alpha = \pi$. The frames are $D \in [-0.6, 0.6]$ and $T \in [0, 300]$. The two vertical broken lines indicate the impact parameter interval, which is magnified in figure 4.

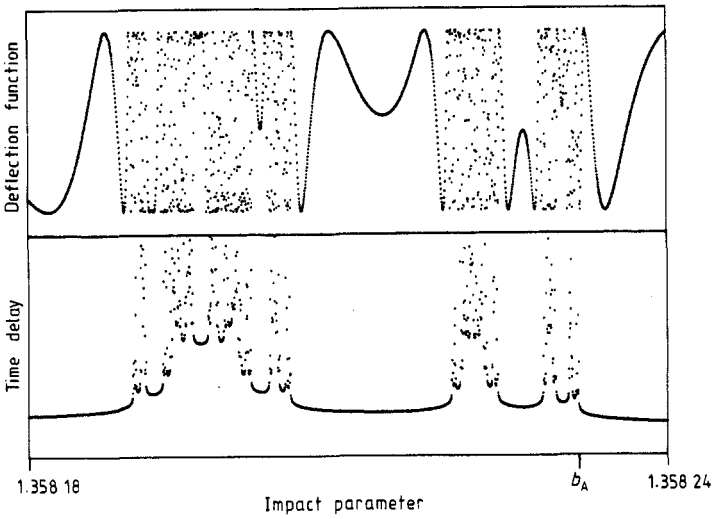

Figure 4. Magnification of figure 3.

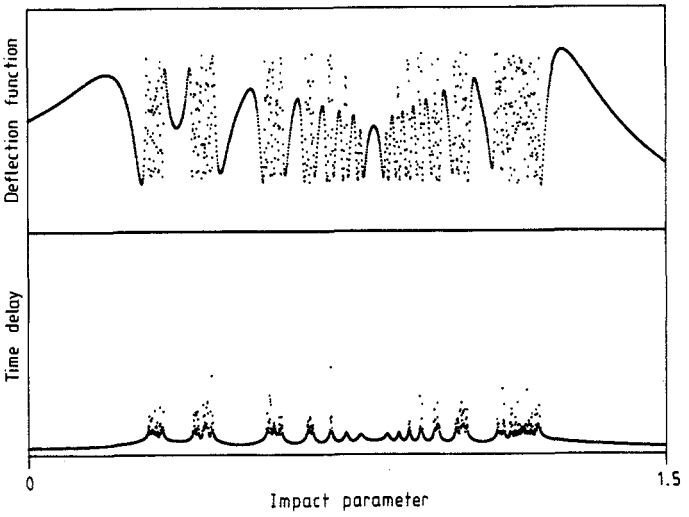

Figure 5. The same as figure 3 for energy $E = 0.05$.

In figures 3 and 4 we see an infinite sequence of singularity clusters becoming smaller to the right in a geometrical progression. The accumulation point of this sequence is $b_A = 1.358\,231\,66\ldots$. These clusters are intervals of the impact parameter, which contain an uncountable number of discontinuous changes of the deflection function and corresponding infinities of the time delay function. For $|b| > b_A$ and for $|b| < 1.3577$ the deflection function is regular. The magnification of figure 3 around b_A, see figure 4, looks similar in its coarse structure to figure 3. In detail, the clusters become more densely filled with substructures similar to the structures of larger scales. In the limit $b \to b_A$ we find exact self-similarity. On any scale there appear new smaller intervals where the functions D and T are smooth. The occurrence of a fractal Cantor set of singularities in the deflection function can be taken as a preliminary criterion

for scattering chaos. Figure 5 shows that at energy $E = 0.05$ the chaos has spread over a larger impact parameter range.

4. Invariant manifolds of the periodic orbit γ

Now we have to establish a relation between the singularities of D and the stable and unstable manifolds W^s and W^u of the periodic orbit γ. In figure 6 we see the Poincaré plot of γ, W^s, W^u together with some quasiperiodic KAM lines around the elliptic point P_e. Out of the infinite number of tendrils of W^s and W^u we have plotted only some tendrils of W^s and only a short piece of W^u. The symmetry of the Hamiltonian (2) implies that W^u can be obtained by reflecting W^s in the line $\dot{\rho} = 0$.

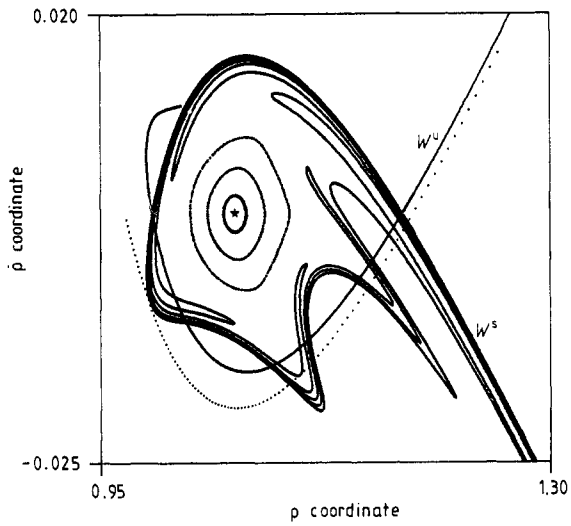

Figure 6. The Poincaré plot in the $\rho/\dot{\rho}$ plane $z = 0$. $\dot{z} > 0$ shows the elliptic fixed point P_e (marked by a star), some KAM lines around P_e, the invariant manifolds W^s, W^u of the hyperbolic point P_h and the transport image of the asymptotic line $\alpha = \pi$, $b > 0$ (dotted). The axes are ρ (horizontal) and $\dot{\rho}$ (vertical).

All tendrils of W^s outside W^u—except the first few ones— extend into the asymptotic region $\rho \to \infty$. Conversely, scattering trajectories starting on the asymptotic parts of W^s will be captured by γ thus forming singularities of D and T. The existence of homoclinic intersections between W^s and W^u implies the existence of hyperbolic invariant sets and Smale horseshoes in M. Furthermore, there are infinitely many periodic orbits and the set of non-periodic localised orbits is uncountable. All these orbits have their own stable and unstable manifolds reaching out to infinity between the tendrils of W^s and W^u. If we scan the uncountable set of stable manifolds of these localised orbits transversally (e.g. by varying b for fixed α and E) we find a one-dimensional Cantor set. This explains the fractal structures of figures 3-5.

Because the singularity set has Lebesgue measure zero, we do not hit the singularities exactly in numerical computations or in actual scattering experiments. What we see is a discontinuity of the scattering angle when the initial condition crosses a stable manifold of a localised orbit. A single discontinuity can be observed already in

rotationally symmetric potentials (orbiting effect). However, to find a whole Cantor set of singularities a non-integrable potential with homoclinic structures is necessary.

Now let us consider the motion of a scattering trajectory S which starts close to the stable manifold of a localised orbit Γ_1. At first, it will be attracted by this orbit. After staying there for some time it will be repelled away along the unstable manifold of Γ_1. Now S can either return to infinity or visit another localised orbit Γ_2 via some heteroclinic connection. There it has to decide again between escaping and remaining inside the potential for another few turns. If S starts with an appropriate impact parameter it can move inside the potential for an arbitrarily long time and it comes close to various localised orbits in any succession before it esccapes to infinity.

The behaviour of trajectories in position space is further illustrated in figure 7. Part (a) shows the periodic trajectory γ oscillating back and forth over the saddle of the potential. In numerical computations it is impossible to start a scattering trajectory exactly on W^s. To show the capture of a scattering trajectory by a localised periodic orbit, in part (b) a scattering trajectory is launched with an impact parameter value very close to b_A and therefore this trajectory starts very close to W^s. Accordingly, the scattering trajectory becomes attracted by γ and makes many turns along γ. After a few revolutions along γ we have stopped the orbit, whereas the actual numerical trajectory finally goes off to infinity again. In parts (c) and (d) we see two trajectories with $b > b_A$. The initial values are close to W^s and the trajectories come close to γ and make a few turns along γ before they go out again to infinity. These scattering trajectories do not cross the orbit γ. Because the initial conditions lie outside the singular region, the trajectories vary continuously when the initial condition b is changed. The two trajectories in (c) and (d) have essentially the same shape. Parts (e) and (f) show two trajectories with $b < b_A$. Also here the initial conditions are close to W^s and the scattering trajectories are first attracted by γ and make a few turns along γ. Because now $b < b_A$, these trajectories cross the orbit γ and enter the interior part of the potential. Here the motion is extremely sensitive to small changes of the

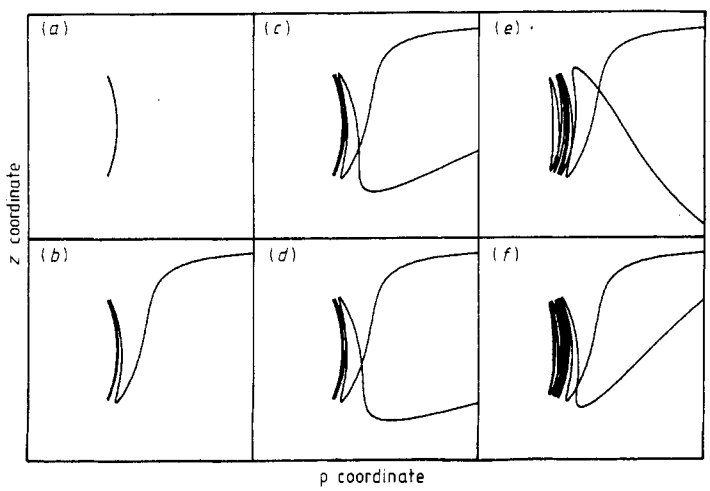

Figure 7. Six trajectories in position space for $E = 0.079$. Part (a) shows the periodic orbit γ. Parts (b)-(f) show scattering trajectories with incoming asymptotes $\alpha = \pi$ and b as follows: (b) 1.358 231 66; (c) 1.358 231 74; (d) 1.358 231 75; (e) 1.358 231 64; (f) 1.358 231 65. In each frame the ρ coordinate (horizontal) ranges from 0 to 3 and the z coordinate (vertical) ranges from -1.5 to $+1.5$.

initial conditions, which causes the discontinuous dependence of the final asymptotes on the initial conditions.

The dynamics on the hyperbolic invariant set is equivalent to a shift of symbolic sequences. Thus captured orbits can realise infinite random sequences whereas scattering orbits trace out finite sequences only. (For a more detailed discussion of this point see Jung and Scholz (1987).)

Next we turn our attention to the dotted curve in figure 6. To this end we introduce the transport map τ: $\mathcal{A} \to F$ from the asymptotic α/b plane $\mathcal{A}$ to the Poincaŕe plane F. If we follow a trajectory starting at $P_1 \in \mathcal{A}$ until it pierces the Poincaré plane F for the first time in $P_2 \in F$, say, then $P_2 = \tau(P_1)$. Not all points $P \in \mathcal{A}$ have an image $\tau(P)$. For example, any trajectory starting with $\alpha > \pi$, $|b| \gg 1$ will never hit the plane F.

Now consider the asymptotic segment

$$K = \{(\alpha, b):\ \alpha = \pi,\ 1.3565 < b < 1.3585\}.$$

The dotted curve in figure 6 is $K' = M(\tau(K))$, where M is the Poincaré map defined in § 2 (the image $\tau(K)$ would be a tiny segment outside the frame of figure 6). Actuallly we have chosen 100 points evenly spaced between $b = 1.3565$ and $b = 1.3585$ and plotted their images. The rightmost point on the dotted curve corresponds to $b = 1.3585$. Comparing figures 3 and 4 with figure 6 we find that the intersection $W^s \cap K'$ indicates the boundaries of the singularity clusters. Thus a correspondence has been found between the singularity structure of the deflection function and the stable manifold of the periodic orbit γ. The fact that in figures 3 and 4 much more singular points are seen than in $W^s \cap K'$ has a simple explanation: in figure 6 only a few tendrils are drawn and most of the singularities in figures 3 and 4 are caused by the stable manifolds of further localised orbits. Close to $b = 1.3568$ the dotted curve just misses intersecting W^s (see figure 6). Accordingly, the functions D and T do not show a genuine singularity there. However, close to this value of b the deflection function oscillates strongly and the time delay is significantly large.

5. Higher-dimensional structure of the singularity set

So far we have treated the case $\alpha = \pi$. Next it would be useful to get an overview of the singularity structure in the three-dimensional set (α, b, E) of all incoming asymptotes.

First we fix the energy at $E = 0.079$ again to look for the singularities in $\mathcal{A}$ contained in a very narrow annullus (see figure 8). On this scale the fractal structure of the singularity ring cannot be resolved. However, the following main features are observed. For $\alpha \neq \pi$ the functions $D(b)$ and $T(b)$ are no longer symmetric. For $|\alpha - \pi| > 0.5$ we have no singularities at all. For these directions the particle misses entering the chaotic region via P_S. Therefore, the scattering cannot be influenced by unstable localised orbits.

To investigate the global structure of τ we have chosen five radial segments A, B, C, D, E which intersect the ring transversally. The corresponding images A', B', C', D', E' under $M \circ \tau$ are shown in figure 9. The transport map turns out to be discontinuous along the cut $\alpha = \pi$, $b > 0$. The transversality $\dot{z} > 0$ is lost at infinity when b is held fixed and α is varied from $\pi - \varepsilon$ to $\pi + \varepsilon$. As a consequence, one piercing through the Poincaré plane is lost and $A' = M(E')$.

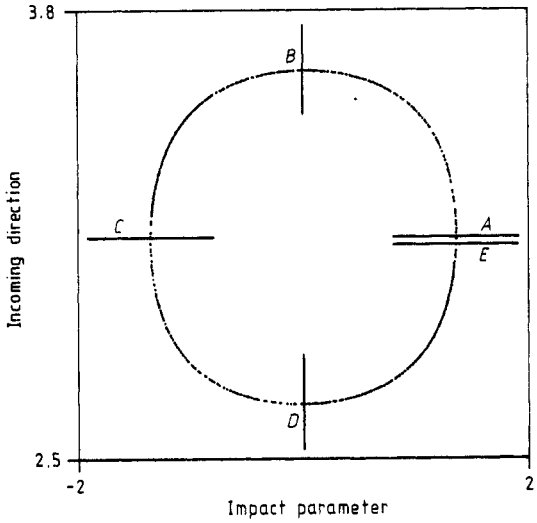

Figure 8. Asymptotic plane of incoming direction α (vertical axis) and impact parameter b (horizontal axis) for $E = 0.079$. The thin annullus indicates the singularities of $D(\alpha, b)$ and $T(\alpha, b)$. The straight lines A, B, C, D, E will be mapped into the Poincaré plane F.

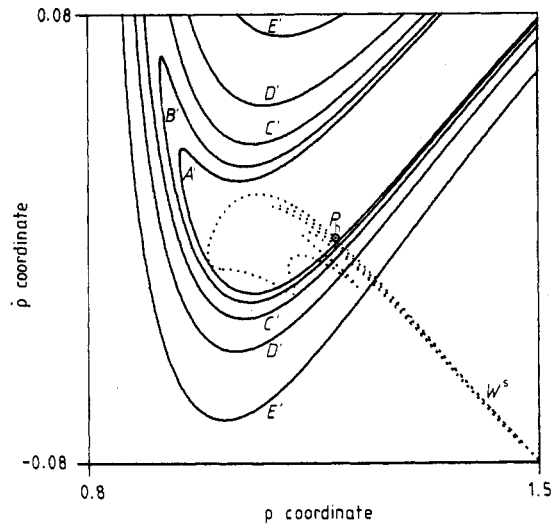

Figure 9. Images of the lines A, B, C, D, E from figure 8 under the map $M \circ \tau$ in the Poincaré plane F. In addition a part of one branch of the stable manifold W^s of the fixed point P_h (denoted by a small circle) is shown.

The transport map is not defined in a small simply connected region near $\alpha = \pi$, $b = 0$. Therefore the domain of τ without the cut is homeomorphic to a rectangle. Under $M \circ \tau$ this rectangle is mapped onto the strip between A' and E'.

Instead of transporting the asymptotic coordinate lattice into F to find intersections with W^s, one can transport W^s backwards in time into $\mathscr{A}$ to look for boundaries of singularity clusters. This defines an inverse transport map τ^{-1}. If $x \in F$ has an inverse Poincaré image $M^{-1}(x)$ then $\tau^{-1}(x) = \tau^{-1}(M^{-1}(x))$. Therefore, to get $\tau^{-1}(W^s)$ it is

sufficient to transport an arc $c=(P_1, P_2)\subset W^s$ where $P_2=M^{-1}(P_1)$. In figure 10 we have plotted 10 000 points of $\tau^{-1}(W^s)=\tau^{-1}(c)$ for $E=0.05$. At this energy the tendrils of W^s appearing in $\mathscr{A}$ are better resolved than for $E=0.079$. The singular points on the line $\alpha=\pi$, $b>0$ can be identified with the boundaries of singularity clusters in figure 5.

In figure 11 we present the scattering singularities in the E/b plane for $\alpha=\pi$ fixed. Notice that the singularities in the line $E=0.05$ are contained in figures 5 and 10 too and that there are no singularities outside the interval (E_S, E_M). Taken together, figures 10 and 11 give some impression of the complicated way in which the leaves of the

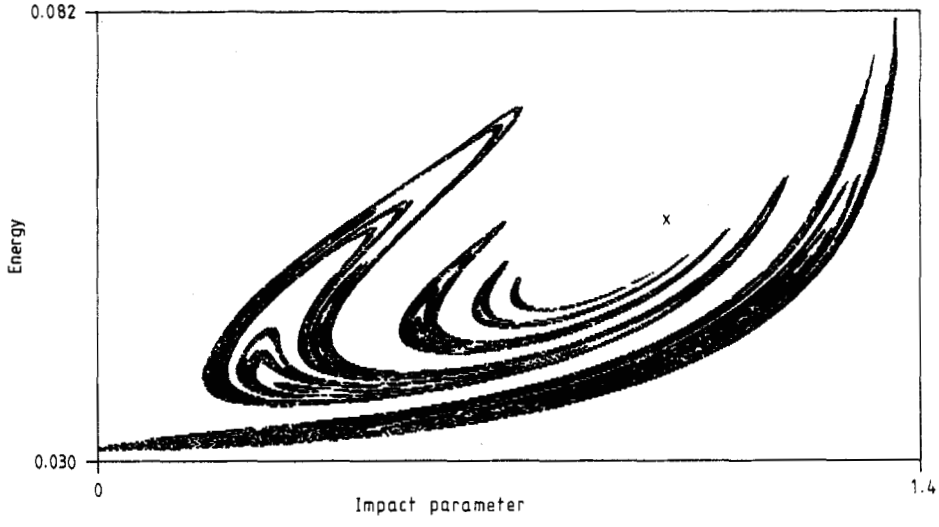

Figure 10. Intersection of W^s with the asymptotic α/b plane for $E=0.05$.

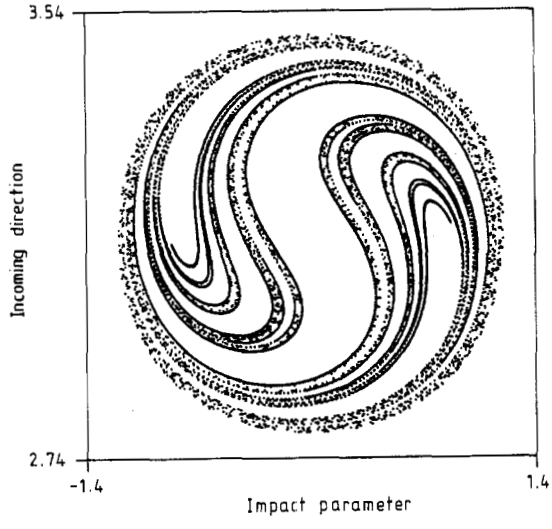

Figure 11. Singularities of D and T in the E/b plane for $\alpha=\pi$. The cross indicates the thalweg singularity.

fractal singularity set are connected and whirled around in the three-dimensional asymptotic space.

In figure 11 there is an additional exceptional point marked by a cross. This singularity, which is completely different in nature from the singularities discussed so far, is related to the thalweg of the potential (3). If a particle starts exactly at the cross it will move through the origin along the thalweg. However, if the particle starts not quite exactly at the cross it will be reflected near the origin.

6. Conclusions

Hyperbolic invariant sets constitute the basic structure of chaos in scattering systems as well as in bound systems. Nevertheless, there is an essential difference in the appearance of chaos in these two cases. In bound systems trajectories lying in the neighbourhood of the hyperbolic set will be influenced by it for an unlimited time, thereby becoming chaotic themselves. Being surrounded by localised chaotic orbits the hyperbolic set cannot be observed in isolation.

In contrast, in chaotic scattering systems the hyperbolic invariant set created by unstable localised orbits casts a shadow into the asymptotic region. As a consequence, there are uncountably many incoming asymptotes which are eventually captured. For $t \to +\infty$ they show chaotic or periodic behaviour. However, the measure of the corresponding set of initial conditions is zero in the asymptotic space (α, b, E). On the other hand, proper scattering orbits whose motion becomes trivial for $t \to -\infty$ and for $t \to +\infty$ feel the non-integrable potential for a finite time only. Therefore, though single scattering orbits may be arbitrarily complicated, they never show real chaos. But the deflection function of these non-chaotic trajectories helps to reveal the basic building blocks of localised chaos in a more direct and pure way than bound chaotic motion is able to do.

References

Agmon N 1982 *J. Chem. Phys.* **76** 1309-16
Braun M 1970 *J. Diff. Eq.* **8** 294
Churchill R C, Pecelli G and Rod D L 1979 *Stochastic Behaviour in Classical and Quantum Hamiltonian Systems* ed G Casati and J Ford (Berlin: Springer) pp 76-136
Contopoulos G and Vlahos L 1975 *J. Math. Phys.* **16** 1469-74
Dragt A J and Finn J M 1976 *J. Geophys. Res.* **81** 2327-40
Eckhardt B 1988 *Europhys. Lett.* **5** 107
Eckhardt B and Aref H 1988 *Phil. Trans. R. Soc.* in press
Eckhardt B and Jung C 1986 *J. Phys. A: Math. Gen.* **19** L829-33
Fitz D E and Brumer P 1979 *J. Chem. Phys.* **70** 5527-33
Gottdiener L 1975 *Mol. Phys.* **29** 1585-95
Jung C and Scholz H-J 1987 *J. Phys. A: Math. Gen.* **20** 3607-17
Noid D W, Gray S K and Rice S A 1986 *J. Chem. Phys.* **84** 2649-52
Petit J M and Henon M 1986 *Icarus* **66** 536-55
Rankin C C and Miller W H 1971 *J. Chem. Phys.* **55** 3150
Schlier C G 1983 *Chem. Phys.* **77** 267-75